Meccanica (2016) 51:2203–2214
DOI 10.1007/s11012-015-0349-z

Double resonance capture of a two-degree-of-freedom oscillator coupled to a non-ideal motor

P. J. P. Gonçalves · M. Silveira · E. A. Petrocino · J. M. Balthazar

Received: 3 December 2014 / Accepted: 10 December 2015 / Published online: 15 December 2015

Abstract This work presents the development of a discrete parameter model consisting of a concentrated mass which is supported by a set of springs and dampers positioned in two orthogonal directions, such that the mass can move horizontally and vertically in a plane. A non-ideal motor is attached to the mass such that the phenomenon of resonance capture can occur. Resonance capture occurs in structures with low damping which are attached to rotating machines with limited power supply. When resonance capture occurs, the mean angular velocity of the motor remains constant and the displacement of the structure increases. An investigation on the influence of the two orthogonal resonance frequencies is presented. It was found that this model can illustrate the dynamics of a more complex structure consisting of a portal frame coupled to a non-ideal unbalanced motor. Experimental tests are used to support numerical simulations and the analytical model.

Keywords Non-ideal motor · Sommerfeld effect · Resonance capture

P. J. P. Gonçalves (✉) · M. Silveira · E. A. Petrocino · J. M. Balthazar
Department of Mechanical Engineering, São Paulo State University - UNESP, 17033-360 Bauru, SP, Brazil
e-mail: paulo.jpg@feb.unesp.br

1 Introduction

The study of interaction between motors and structures is not new. Probably the first to notice the dynamics between motors and structures was A. Sommerfeld [15]. He proposed an experiment of a motor mounted on a flexible wooden table and observed that the energy supplied to the motor was converted in the form of table vibration, instead of being converted to increase angular velocity of the motor. This observation was used to explain a class of motors called non-ideal energy sources. Latter, Laval was the first to perform an experiment with a steam turbine to observe that quick passage though critical speed would reduce significantly the levels of vibration when compared to steady state excitation [1].

The non-ideal energy source have influence on the system near the resonance regime. Considering a DC motor, usually the angular velocity increases according to the power supplied to the source. However, due to the Sommerfeld effect, near the resonance, with additional energy the mean angular velocity of the DC motor remains unchanged until it suddenly jumps to a much higher value upon exceeding a critical input power. Simultaneously, the amplitude of oscillations of the excited system jumps to a much lower value. Before the jump, the non-ideal oscillating system can not pass through the resonance frequency of the system, or requires an intensive interaction between the vibrating system and the energy source to be able to do so [7].

Considering the analysis of such systems, Palacios et al. [12] applied the Bogoliubov Averaging Method to the study of the vibrations of an elastic foundation, forced by a non-ideal energy source. They considered a model consisting of a planar portal frame with quadratic nonlinearities and internal resonance 1:2, supporting a direct current motor with limited power. Quinn et al. [13] presented an approximated method to identify which sets of initial conditions lead to resonance capture and in [14] the author presents a complete study of the conditions of resonance capture in a three-degree-of-freedom (DOF) system.

Reference [16] considers the dynamical behavior of a 2-DOF in the presence of a 1:1 resonance between two components with non-linear inertial coupling. Kerschen et al. [9] reported an experimental study of transient resonance capture that may occur in a system of two coupled oscillators with essential nonlinearity. It is shown that during transient resonance capture the two oscillators are in a state of resonance, the frequency of which varies with time. Lee et al. [11] studied the dynamics of a 2-DOF nonlinear system consisting of a grounded linear oscillator coupled to a light mass by means of an essentially nonlinear (nonlinearizable) stiffness. They have considered first the undamped system and performed a numerical study based on non-smooth transformations to determine its periodic solutions in a frequency-energy plot. Bishop and Galvanetto [2] considered the behavior of a mechanical oscillator with cubic nonlinearity subjected to a forcing excitation whose frequency remains constant while the amplitude is ramped. They have found that the reduced level of forcing at the initial stages of ramping produces a delay in bifurcational events when compared to the constant sinusoidally forced counterpart. In ref. [5], a nonlinear control method is studied based on the phenomenon of mode saturation which is applied to a portal frame support and unbalanced motor with limited power. An alternative method is analised in ref. [4] which consists in the energy transfer of a structure (cantilever beam) with a non-ideal motor using linear electromechanical vibration absorber (LEVA) and a nonlinear electromechanical vibration absorber (NEVA).

Also, in terms of continuous systems with coupled motors, Krasnopolskaya [10] studied an infinite plate immersed in an acoustic medium. The plate was subject to a point excitation by an electric motor of limited power-supply, and it was shown that chaos might occur in the system due to the feedback influence of waves in the infinite hydro-elastic subsystem in the regime of motor shaft rotation.

In this work, a 2-DOF discrete (lumped) parameter model of a mass vibrating in a plane is presented in Sect. 2 and is used to investigate the phenomenon of resonance capture. The model analogy presented in [7] is extended to a 2-DOF system in Sect. 3. In Sect. 4, different cases are studied varying the ratio of vertical and horizontal stiffness to identify regions in which double resonance capture occurs. Section 5 presents a brief discussion of results obtained by a finite element method that helps understand the behavior of a continuous structure, and Sect. 6 contains experimental results showing the effect of structural modifications on the resonance capture. Finally, conclusions are given in Sect. 7.

2 System modeling

The system considered in this work is presented in Fig 1, which consists of a mass M supported by springs and viscous dampers in two orthogonal directions (x and y). The spring constants are defined by k and the damping coefficients by c. The subscripts x and y indicated the displacement direction. Attached to the mass, there is a rotating motor, with unbalanced mass m at a distance r from the center of the motor shaft. The motor shaft has moment of inertia defined by J_0.

The equations of motion of an electrical motor attached to a structure are developed based on

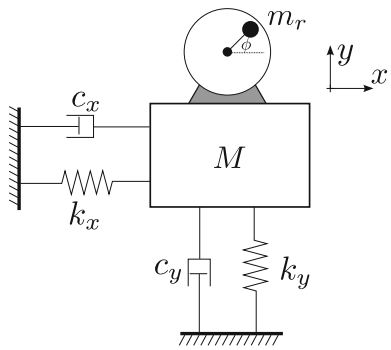

Fig. 1 Discrete parameter system with two-degree-of-freedom and coupled non-ideal unbalanced motor

Lagrange equations. The model is related to an experimental device described in Sect. 6.

2.1 Energy equations

To apply Hamilton's principle, expressions for the kinetic and potential energy need to be written in terms of the unknown degrees of freedom. The kinetic energy is defined as

$$T = \frac{1}{2}M\dot{x}^2 + \frac{1}{2}M\dot{y}^2 + \frac{1}{2}J_0\dot{\phi}^2 + \frac{1}{2}m\left(\dot{x}_m^2 + \dot{y}_m^2\right) \tag{1}$$

The term J_0 defines the motor shaft moment of inertia, and the terms $x_m = x + r\cos\phi$ and $y_m = y + r\sin\phi$ define the position of the motor's unbalanced mass m, with r being the distance of this mass to the motor's center of rotation. Then, Eq. 1 can be written as

$$\begin{aligned} T = &\frac{1}{2}(M+m)\dot{x}^2 + \frac{1}{2}(M+m)\dot{y}^2 \\ &+ \frac{1}{2}\left(J_0 + mr^2\right)\dot{\phi}^2 + mr\dot{\phi}(\dot{y}\cos\phi - \dot{x}\sin\phi) \end{aligned} \tag{2}$$

If the gravity potential energy is neglected, then the system's potential energy is simply

$$U = \frac{1}{2}k_x x^2 + \frac{1}{2}k_y y^2 \tag{3}$$

2.2 Equations of motion

The equations of motion of the system are obtained by writing the Lagrangian, $L = T - U$, and first-order stationary conditions in the form of Hamilton's equation

$$\frac{d}{dt}\left(\frac{\partial L}{\partial \dot{q}_i}\right) - \left(\frac{\partial L}{\partial q_i}\right) = F_i \tag{4}$$

in which F_i are the non-conservative forces, which are the viscous damping forces $F_x^{damp} = -c_x\dot{x}$, $F_y^{damp} = -c_y\dot{y}$ and the torque $\mathfrak{M}$ applied to the motor.

Applying Eqs. 2 and 3 into 4, it is possible to obtain the cart's equations of motion for x and y directions

$$(M+m)\ddot{x} + k_x x + c_x\dot{x} = mr\left(\dot{\phi}^2\cos\phi + \ddot{\phi}\sin\phi\right) \tag{5}$$

$$(M+m)\ddot{y} + k_y y + c_y\dot{y} = mr\left(\dot{\phi}^2\sin\phi - \ddot{\phi}\cos\phi\right) \tag{6}$$

and the equation of motion for the unbalanced mass

$$\left(J_0 + mr^2\right)\ddot{\phi} = mr(\ddot{x}\sin\phi - \ddot{y}\cos\phi) + \mathfrak{M}\left(\dot{\phi}\right) \tag{7}$$

Equations 5, 6 and 7 can be conveniently written in terms of the parameters

$$\begin{aligned} \omega_x &= \sqrt{\frac{k_x}{M+m}}, \quad \omega_y = \sqrt{\frac{k_y}{M+m}} \\ \xi_x &= \frac{c_x}{2(M+m)\omega_x}, \quad \xi_y = \frac{c_y}{2(M+m)\omega_y} \\ \mu_1 &= \frac{mr}{M+m}, \quad \mu_2 = \frac{mr}{J_0 + mr^2} \end{aligned}$$

such that

$$\ddot{x} + \omega_x^2 x + 2\xi_x\omega_x\dot{x} = \mu_1\left(\dot{\phi}^2\cos\phi + \ddot{\phi}\sin\phi\right) \tag{8}$$

$$\ddot{y} + \omega_y^2 y + 2\xi_y\omega_y\dot{y} = \mu_1\left(\dot{\phi}^2\sin\phi - \ddot{\phi}\cos\phi\right) \tag{9}$$

$$\ddot{\phi} = \mu_2(\ddot{x}\sin\phi - \ddot{y}\cos\phi) + \mathfrak{M}\left(\dot{\phi}\right)/\left(J_0 + mr^2\right) \tag{10}$$

2.3 Model order reduction

The order of the equations describing the motion of the system (Eqs. 8, 9 and 10) are reduced by the use of the state variables $q_1 = x$, $q_2 = y$, $q_3 = \phi$, $q_4 = \dot{x}$, $q_5 = \dot{y}$ and $q_6 = \dot{\phi}$, such that the velocities are re-written as

$$\dot{q}_1 = q_4 \tag{11}$$

$$\dot{q}_2 = q_5 \tag{12}$$

$$\dot{q}_3 = q_6 \tag{13}$$

The accelerations can be calculated by solving the linear system of differential equations

$$\begin{aligned} &\begin{bmatrix} 1 & 0 & -\mu_1\sin\phi \\ 0 & 1 & \mu_1\cos\phi \\ -\mu_2\sin\phi & \mu_2\cos\phi & 1 \end{bmatrix} \begin{bmatrix} \ddot{x} \\ \ddot{y} \\ \ddot{\phi} \end{bmatrix} \\ &= \begin{bmatrix} -\omega_x^2 x - 2\xi_x\omega_x\dot{x} + \mu_1\dot{\phi}^2\cos\phi \\ -\omega_y^2 y - 2\xi_y\omega_y\dot{y} + \mu_1\dot{\phi}^2\sin\phi \\ \mathfrak{M}(\dot{\phi})/(J_0 + mr^2) \end{bmatrix} \end{aligned} \tag{14}$$

in which $\dot{q}_4 = \ddot{x}$, $\dot{q}_5 = \ddot{y}$ and $\dot{q}_6 = \ddot{\phi}$. The solution of the system shown in equation 14 is presented in the appendix.

2.4 Non-ideal motor

To define a limited power, or non-ideal, motor, two parameters are used to represent the torque as a function of the angular velocity, given by

$$\mathfrak{M}(\dot{\phi}) = M_0\left(1 - \frac{\dot{\phi}}{\Omega_0}\right) \tag{15}$$

in which M_0 and Ω_0 are constants of the motor, the first related to static torque and the second related to zero torque.

Equation 15 is represented by the curve shown in Fig. 2 where the torque $\mathfrak{M}$ is a function of the angular velocity $\dot{\phi}$. For values of angular velocity equal to Ω_0, the torque reduces to zero, and when the angular velocity is zero, the torque is maximum and equal to M_0.

3 Model analogy

A ramp model analogy was presented by [7], which illustrate the phenomenon of resonance capture by the use of a wheel climbing a ramp. When considering a motor mounted over a rigid base, the motor acceleration is defined by

$$\ddot{\phi}\left(J_0 + m_r r^2\right) = M_0\left(1 - \frac{\dot{\phi}}{\Omega_0}\right) \tag{16}$$

It is possible to develop a model analogy for the system described in Eq. 16 using the system shown in Fig. 3. In this figure, a wheel must climb a ramp to reach a certain level of energy defined by Ω_0. When considering a motor with resistive torque, the angular acceleration is no longer constant and decreases as the angular velocity increases and the rate of changing in the angular velocity is no longer linear.

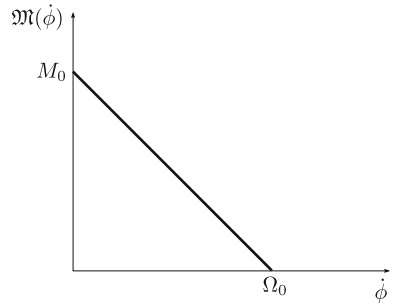

Fig. 2 Motor torque characteristic curve

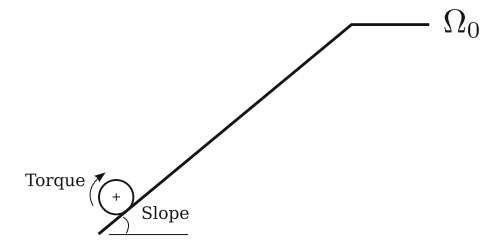

Fig. 3 Analogy by a wheel climbing a ramp, motor with no resistive torque (from ref. [7])

When the motor is mounted on a flexible base, it is clear in Eq. 10 that the angular acceleration is also a function of the cart motion. Also, the motion of the cart is a function of the acceleration and angular velocity of the motor. The system shown in Fig. 4 represents an analogy when the motor is mounted on a flexible base.

In this case, the ramp path is modified by the cart resonance frequency ω_0. The resonance frequency is represented by the valley in the ramp path. The depth and the width of the valley in the ramp are related to the amplitude of the motion of the cart, and in some cases the wheel can get stuck inside the valley in the ramp path.

For the system with two resonance frequencies, a similar analogy is presented in Fig. 5. Now the ramp path presents two valleys, one related to the resonance frequency in the x direction (ω_x) and another related to the resonance frequency in the y direction (ω_y). Depending in the ratio ω_x/ω_y, these two valleys can be far apart, resulting in double resonance capture, or they can be close to each other and interact, resulting in single capture. The dynamic factors controlling this

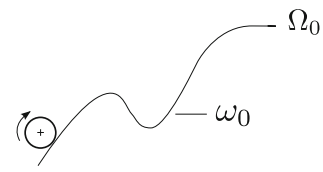

Fig. 4 Analogy of the resonance frequency in the ramp path, ω_0 is the resonance frequency and Ω_0 is the desired angular frequency (from ref. [7])

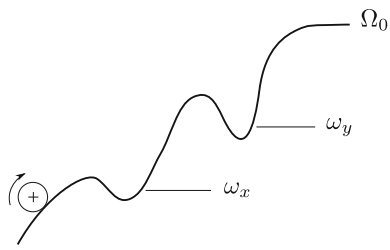

Fig. 5 Analogy of the resonance frequency in the ramp path, ω_x is the resonance frequency in the x direction, ω_y is the resonance frequency in the y direction and Ω_0 is the desired angular frequency

behavior are explored in the following sections of this paper.

4 Numerical simulations

In this section numerical simulations are performed with the system defined by the first order differential equations developed in the previous sections. The parameters used in the simulations are defined in Table 1

4.1 Stationary condition

This numerical example considers the case of setting the motor angular velocity to a fixed value. The motor is accelerated from rest to a fixed velocity by changing the parameter Ω_0. For instance, when setting $\Omega_0 = 1.1\omega_0$ the motor does not reach the angular velocity $1.1\omega_0$, instead it oscillates with angular velocity ω_0. As a consequence, the additional energy increases the amplitude of the displacement of the cart.

Table 1 System Nominal Parameters

Parameter	Value
Mass M	0.064 kg
Unbalanced mass m	0.0021 kg
Shaft inertia J_0	1e-7 Nm^2
Unbalanced radius r	0.005 m
Motor constant M_0	0.005 Nm
Motor constant Ω_0	Variable
Resonance frequency—ω_x	Variable
Resonance frequency—ω_y	Fixed
Damping ratio ξ_x	Variable
Damping ratio ξ_y	Variable

4.2 Model implementation

The numerical model was implemented using GNU Octave and C language using the GSL (GNU Scientific Library for numerical integration). Both GNU Octave and GSL are freely available. Two different numerical integration algorithms were used. The first is the well known explicit Runge-Kutta method of order (4, 5) used for non-stiff ordinary differential equations. The second is the 5 th order algorithm for stiff ordinary differential equations described in reference [8]. The parameters which are of interest in the simulations are the cart displacement (or velocity) and the motor angular velocity. The motor angular position is a parameter that is confined in the range $[0\ \ 2\pi]$.

For the simulations, the five cases described in Table 2 are considered. In these cases, different ratios of ω_x/ω_y are defined, and ξ_x and ξ_y are calculated accordingly.

4.3 Case 1: $(\omega_x = \omega_y)$

The simulations for case 1 are performed considering that the resonance frequencies ω_x and ω_y are the same. Figure 6 presents the amplitude in both x and y directions as a function of the parameter Ω_0. Results are normalized by the resonance frequency ω_x.

The results shown in Fig. 6a indicate that the resonance capture occurs in both directions and the amplitude in x and y directions are the same. Figure 6b presents the evolution of the angular velocity as a

Table 2 Numerical Simulation Cases

Case number	Parameters		
Case 1	$\omega_x = \omega_y$	$\xi_x = 0.006$	$\xi_y = 0.006$
Case 2	$\omega_x = \frac{1}{2}\omega_y$	$\xi_x = 0.011$	$\xi_y = 0.006$
Case 3	$\omega_x = \frac{1}{\sqrt{2}}\omega_y$	$\xi_x = 0.008$	$\xi_y = 0.006$
Case 4	$\omega_x = \frac{1}{\sqrt{2}}\omega_y$	$\xi_x = 0.0001$	$\xi_y = 0.006$
Case 5	$\omega_x = \frac{1}{\sqrt{2}}\omega_y$	$\xi_x = 0.006$	$\xi_y = 0.0001$

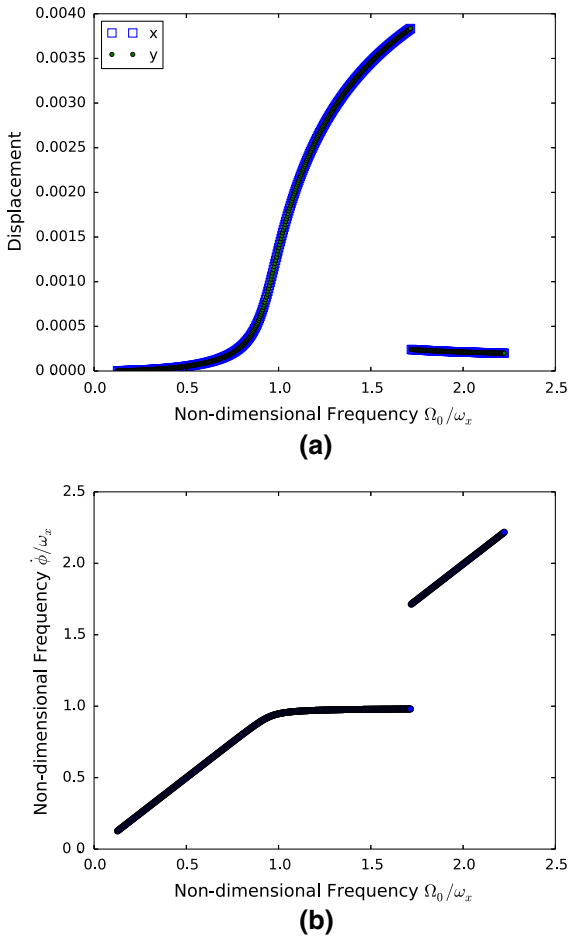

Fig. 6 Displacement amplitude as a function of the parameter Ω_0 (**a**) and angular velocity as a function of Ω_0 (**b**) with $\omega_x/\omega_y = 1$

function of Ω_0. When resonance capture occurs, the angular velocity remains the same.

The hysteresis behaviour was also observed when increasing or decreasing the parameter Ω_0 for different initial conditions. This is observed in the result of fig. 7

4.4 Case 2: $(\omega_x = \frac{1}{2}\omega_y)$

In the simulations for this case, the resonance frequency ω_x is defined by a half of the resonance frequency in the y direction. In this case, for the values of damping considered, the two resonance frequencies are well separated, and for this reason two resonance captures occur. This can be see in Fig. 8a, where the displacement amplitude as a function of Ω_0 is

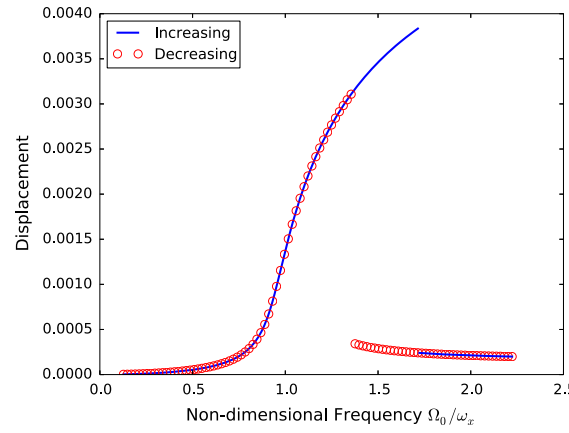

Fig. 7 Displacement amplitude as a function calculated increasing and decreasing the parameter Ω_0

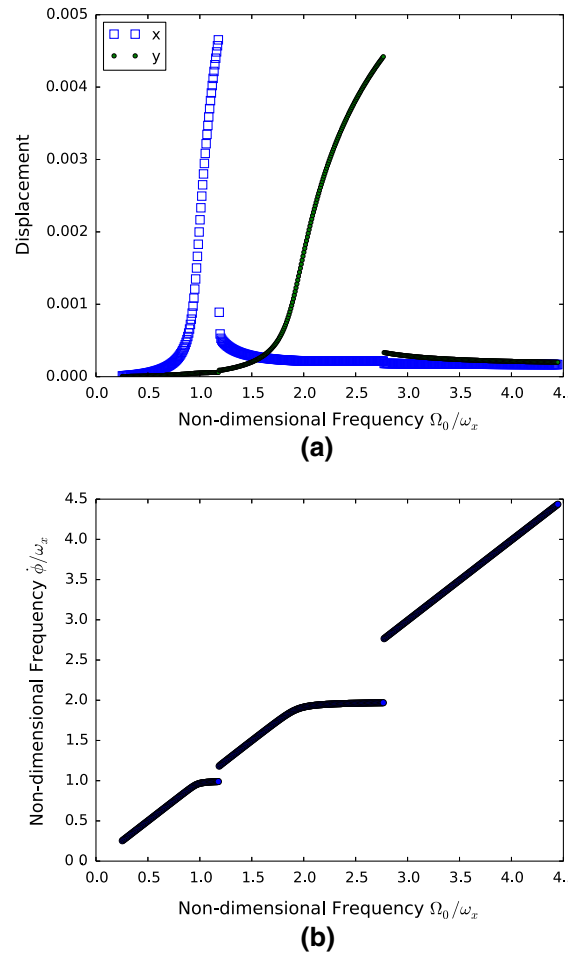

Fig. 8 Displacement amplitude as a function of the parameter Ω_0 (**a**) and angular velocity as a function of the parameter Ω_0 (**b**) with $\omega_x/\omega_y = 1/2$

presented. The two resonance captures also can be seen in the results shown in Fig. 8b for the angular velocity, which remains in the same value during each capture.

4.5 Case 3: $(\omega_x = \frac{1}{\sqrt{2}}\omega_y)$

For the parameters used in the simulations for this case, the resonance frequencies are not well separated such as in case 2. The consequence is that there is an interaction between the resonance frequencies in both directions when the angular velocity passes through these frequencies, even though these frequencies are farther apart than in the previous case. This can be observed in Fig. 9a, with the displacements in x and y directions being influenced by the resonance frequency of each direction. The same influence can be observed in the results of Fig. 9b for angular velocity.

4.6 Case 4: $(\omega_x = \frac{1}{\sqrt{2}}\omega_y)$, low damping $\xi_x \approx 0$

Another interesting situation occurs when damping is reduced to nearly zero in one of the directions. In this simulation case, a small value of damping is assumed in the x direction, such that the displacement amplitude in this direction is much higher than the displacement amplitude in the y direction. There is no resonance capture in the y direction as illustrated in Fig. 10a. The angular velocity shown in 10b also indicates that there is only one capture.

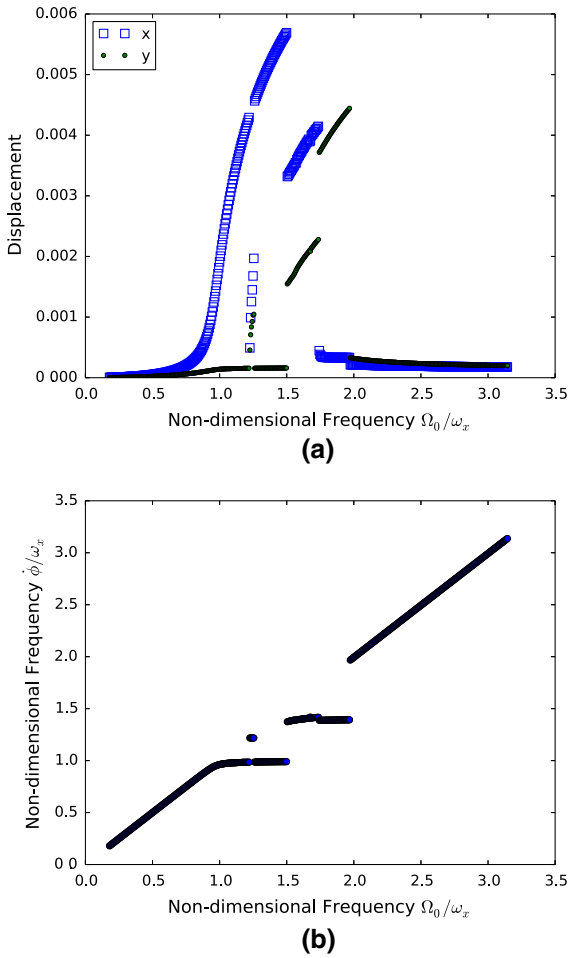

Fig. 9 Displacement amplitude as a function of the parameter Ω_0(**a**) and angular velocity as a function of the parameter Ω_0 (**b**) with $\omega_x/\omega_y = 1/\sqrt{2}$

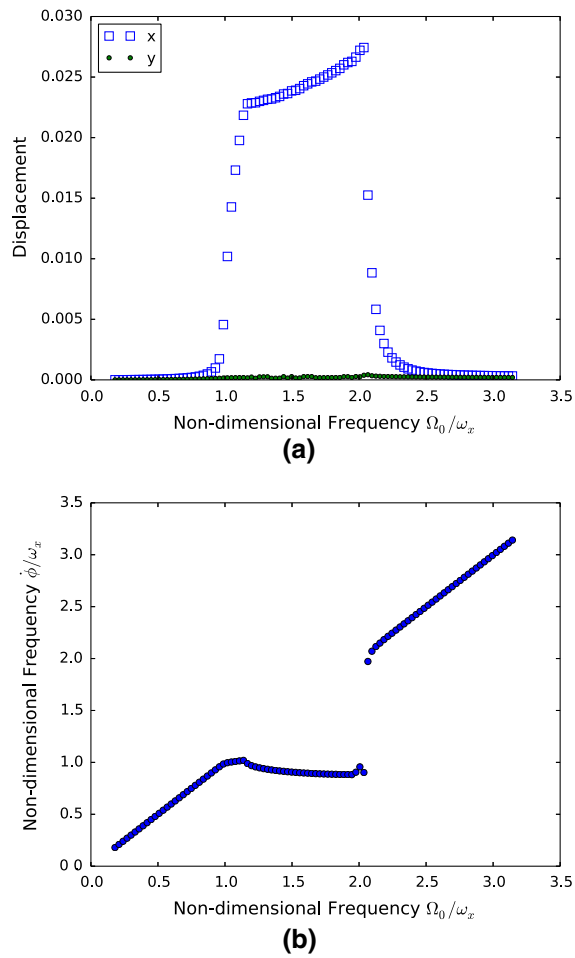

Fig. 10 Displacement amplitude as a function of the parameter Ω_0 (**a**) and angular velocity as a function of the parameter Ω_0 (**b**)

4.7 Case 5: ($\omega_x = \frac{1}{\sqrt{2}}\omega_y$), low damping $\xi_y \approx 0$

Similarly to the simulations presented in case 4, the value of damping in the damper related to the y direction was reduced to a very low value. The system behavior in terms of displacement amplitude and angular velocity as a function of the parameter Ω_0 is shown in Fig. 11a and 11b. Although the displacement in x direction increases at lower frequencies, only displacement in y direction demonstrates resonance capture.

4.8 Sensitivity to M and c

Further simulations were performed to better illustrate the influence of the parameters of the system in the existance of the double resonance capture. Using the parameters of Case 1 ($\omega_x = \omega_y$), a surface showing the displacement as a function of Ω_0 for varying M can be built as in Fig. 12a. The flat portion of this surface represents the resonant capture, and the discontinuity in this surface represents the jump when the system is able to overcome the capture. Although the discontinuity can be seen for a wide range of M, the size of the gap decreases considerably for M up to 0.1 kg, and then decreases at a much lower rate for larger M, as can be observed in Fig. 12b. A similar surface can be built for the displacement as a function of Ω_0 for varying c, showing that the gap decreases at a steady rate for values of c.

The surface for varying M using the parameters of Case 2 ($\omega_x = \frac{1}{2}\omega_y$) is shown in Fig. 13a. Double resonance capture is present for $M < 0.3$. For larger M, only the resonance capture at Ω_0 near ω_y remains. The discontinuity in the surface is very similar to the case in which $\omega_x = \omega_y$, and so is the gap sensitivity for increasing M, as can be seen in Fig. 13b. The surface built for the displacement as a function of Ω_0 for varying c (Fig. 14) shows that the gap at both

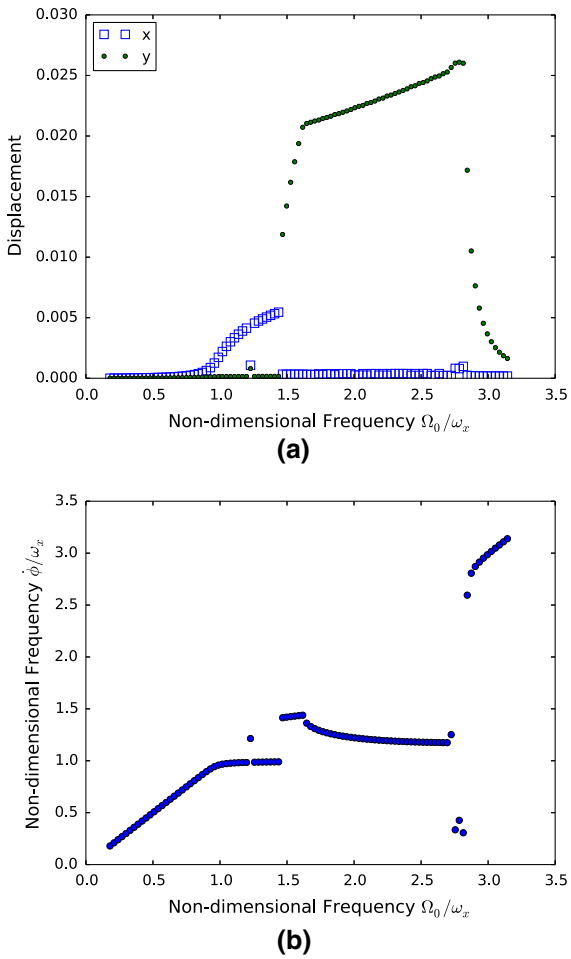

Fig. 11 Displacement amplitude as a function of the parameter Ω_0 (**a**) and angular velocity as a function of the parameter Ω_0 (**b**)

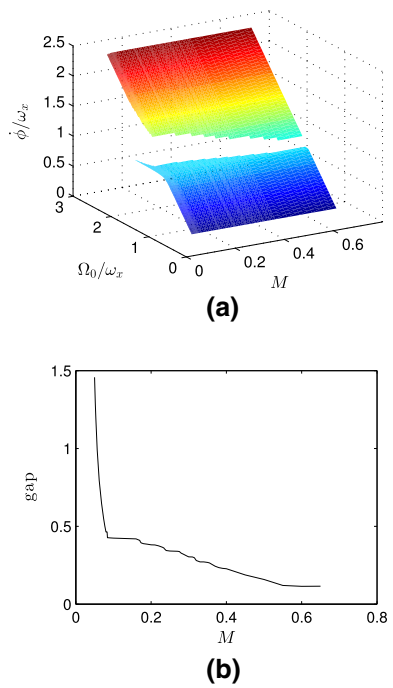

Fig. 12 Displacement as a function of Ω_0 for varying M (**a**) and gap magnitude as function of M (**b**) for $\omega_x = \omega_y$

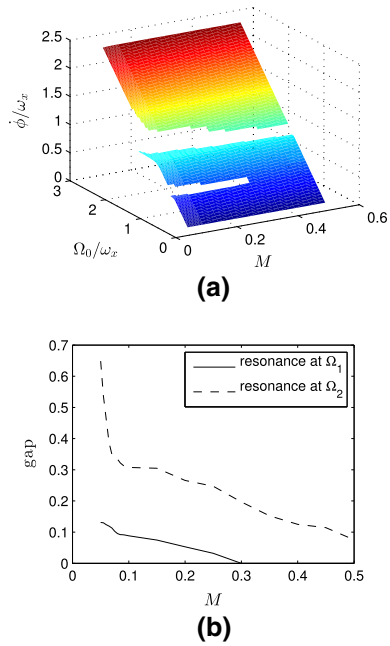

Fig. 13 Displacement as a function of Ω_0 for varying M (**a**) and gap magnitude as function of M (**b**) for $\omega_x = \frac{1}{2}\omega_y$

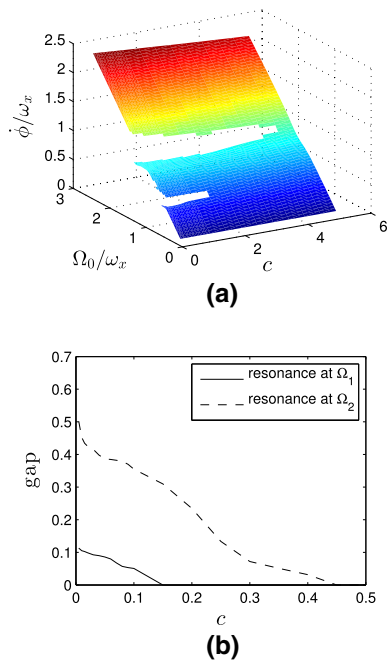

Fig. 14 Displacement as a function of Ω_0 for varying c (**a**) and gap magnitude as function of c (**b**) for $\omega_x = \frac{1}{2}\omega_y$

discontinuities decrease similarly for larger c. With $c > 0.45$, none of the discontinuities remain.

5 Portal frame model

The experimental system considered in this work is a frame structure consisting of a long horizontal beam supported by two shorter vertical beams, as shown sche-matically in Fig. 15. The bending stiffness of the horizontal beam corresponds to k_y of the 2-DOF discrete system shown in Fig. 1, while the equivalent bending stiffness of the two vertical beams corresponds to k_x. Attached to the center of the horizontal beam is a non-ideal electrical DC motor with unbalanced mass, which excites the structure at a frequency determined by its angular velocity.

A finite element model was developed to help understand the dynamics and to determine the natural frequencies and mode shapes of the continuous system, as these are necessary for the correct analysis of the experimental results in the next section. The finite element model was developed using GMSH software [6] for meshing and Calculix Solver, which is based on the theory described in reference [3]. A total of 80 second order beam elements are used to represent the structure. Properties were set using Young's Modulus $E = 193$ GPa and density of 8000 k/m^3. The horizontal and vertical beams have thickness of 1.21×10^{-3} m and width of 24.0×10^{-3} m. The length of the horizontal beam is 0.4 m and the height of the vertical beams is 0.05 m.

Analysis was performed using the Lanczos Method to determine the natural frequencies and mode shapes of the portal frame. The first two mode shapes are shown in Figs. 16 and 17. In the first mode, the horizontal beam has large bending motion, while the

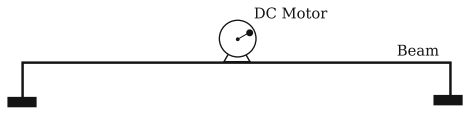

Fig. 15 Schematic representation of the portal frame system with unbalanced motor

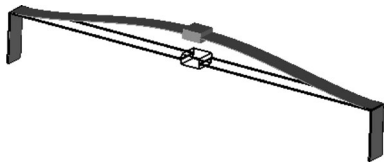

Fig. 16 The first mode shape of the structure, corresponding to 16 Hz

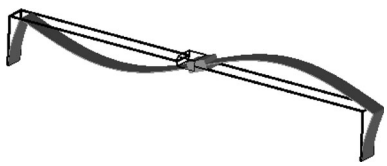

Fig. 17 The second mode shape of the structure, corresponding to 37 Hz

vertical beams have very small motion. In the second mode, all beams present large bending motion.

6 Experimental tests

This section explains the experimental procedure used to verify some of the characteristics investigated by the numerical model studied in this work. The experiment consisted in measuring the voltage at a piezoelectric element positioned as shown in Fig. 18. The voltage at the piezoelectric element corresponds to the level of vibration experienced by the portal frame. The measurements were made in only one point in the structure, as this point presents motion on both modes and can indicate resonance in each mode.

The procedure to obtain the results shown in Fig. 19 were performed by slowly increasing the voltage applied to the DC motor and measuring the voltage produced by the piezoelectric element. The angular

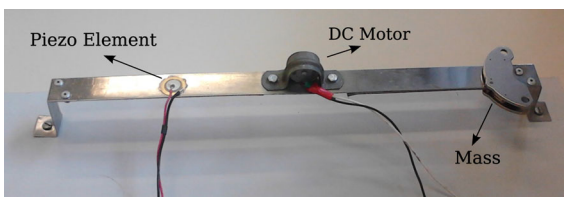

Fig. 18 The experimental apparatus consisting of a portal frame, an unbalanced DC motor, and an additional mass to represent structural modifications. Vibration of the frame is measured using a piezoelectric element

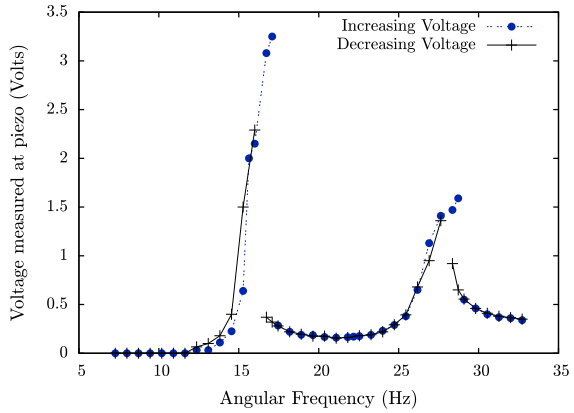

Fig. 19 The voltagem amplitude measured by the piezoelectric element as a function of the angular frequency of the motor. Two situations with increasing and decreasing voltage applied to the motor

frequency of the motor was obtained using the optical sensor illustrated in Fig. 22 of the appendix. After that, a similar procedure was performed by slowly decreasing the voltage applied to the motor. The results of Fig. 19 show the nonlinear behavior with double resonance capture corresponding to the natural frequencies of the two first mode shapes of the portal structure, with each peak corresponding to capture in one mode. It is also possible to observe the jumps when the system escapes capture. These results are in good agreement with what was observed with the discrete system in Sect.4.

6.1 Structural modifications

The structural modifications are performed by adding concentrated mass to some specified positions in the structure. The masses used in the experiments are considerably large compared to the structure of the portal frame, therefore changes can be easily identified. The purpose is not to develop algorithms to quantify structural changes, but to understand the dynamics involved in the system. The chosen locations for positions of these masses are shown in Fig. 20.

The results obtained with structural changes are compared with the baseline conditions of Fig. 19 and are presented in Fig. 21. In the first modification, the mass is positioned at 35 mm from the right edge of the horizontal beam. In the second modification, the mass is positioned closer to the motor, at 160 mm from the horizontal beam right edge.

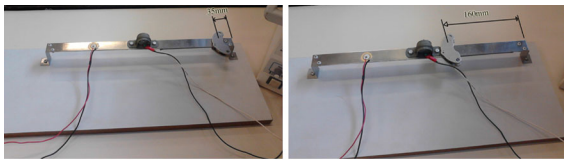

Fig. 20 Positions of the concentrated mass, 35 mm (**a**) and 160 mm (**b**) from the right edge of the horizontal beam

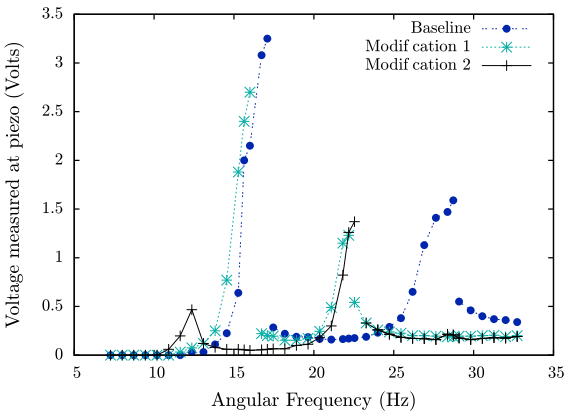

Fig. 21 The voltage amplitude measured by the piezoelectric element as a function of the angular frequency of the the motor. Baseline and two positions for the concentrated mass

The results shown in Fig. 21 indicate that the second resonance frequency is affected by the changes of mass in these two positions, although the modification 1 does not have significant effect on the first resonance frequency. This is explained by the mode shapes shown in Figs. 16, 17. Position 1 is close to a nodal point for the first mode shape, so placing a mass in this position does not have influence on the first resonance peak (16 Hz), related to this mode. However, adding mass at Position 1 does influence the second peak, reducing the resonance frequency from 30 to 23 Hz.

On the other hand, the second position can affect both mode shapes, as it is not close to any nodal point of the mode shapes. This second structural modification has a significant effect on the first peak, as it was not observed resonance capture for the first natural frequency. Still, the effect on the second peak was similar to modification 1.

7 Conclusions

This work presented an analysis of discrete parameter spring-mass-damper free to move in two orthogonal directions which is attached to a non-ideal rotating machine. The system behaves differently according to the values of resonance frequencies in the two orthogonal directions. Depending on the values of these frequencies and the values of damping, resonance capture can occur in both directions, only in one direction, or can not occur.

An experiment was conducted with a structure consisting of a portal frame with an unbalanced DC motor such that two resonance captures could occur for the system. Structure modifications were performed by placing a mass at different positions of the horizontal beam. It was shown that these modifications alter the coupling between the beam and the motor, to the extent that resonance capture can be prevented.

Appendix

The equations of motion in terms of the uncoupled accelerations are given in Eqs. 17, 18 and 19.

$$\begin{aligned}\ddot{x} = &-\frac{\mu_1 \sin(\phi)\mathfrak{M}(\dot{\phi})}{J_1(\mu_1\mu_2 - 1)} \\ &+ \frac{\mu_1\mu_2 \cos(\phi)\sin(\phi)\left(\mu_1 \sin(\phi)\dot{\phi}^2 - F_y\right)}{\mu_1\mu_2 - 1} \\ &+ \frac{\left(\mu_1\mu_2 \cos(\phi)^2 - 1\right)\left(\mu_1 \cos(\phi)\dot{\phi}^2 - F_x\right)}{\mu_1\mu_2 - 1}\end{aligned} \tag{17}$$

$$\begin{aligned}\ddot{y} = &\frac{\mu_1 \cos(\phi)\mathfrak{M}(\dot{\phi})}{J_1(\mu_1\mu_2 - 1)} \\ &+ \frac{\left(\mu_1\mu_2 \sin(\phi)^2 - 1\right)\left(\mu_1 \sin(\phi)\dot{\phi}^2 - F_y\right)}{\mu_1\mu_2 - 1} \\ &+ \frac{\mu_1\mu_2 \cos(\phi)\sin(\phi)\left(\mu_1 \cos(\phi)\dot{\phi}^2 - F_x\right)}{\mu_1\mu_2 - 1}\end{aligned} \tag{18}$$

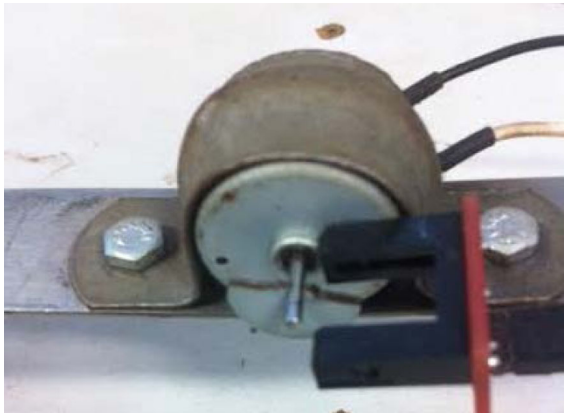

Fig. 22 Optical sensor used to measure the angular velocity in the motor

$$\ddot{\phi} = -\frac{\mathfrak{M}(\dot{\phi})}{J_1(\mu_1\mu_2 - 1)} + \frac{\mu_2\cos(\phi)\left(\mu_1\sin(\phi)\dot{\phi}^2 - F_y\right)}{\mu_1\mu_2 - 1} - \frac{\mu_2\sin(\phi)\left(\mu_1\cos(\phi)\dot{\phi}^2 - F_x\right)}{\mu_1\mu_2 - 1} \tag{19}$$

in which,

$$F_x = \omega_x^2 x + 2\xi_x\omega_x\dot{x} \tag{20}$$

$$F_y = \omega_y^2 x + 2\xi_y\omega_y\dot{y} \tag{21}$$

$$J_1 = J_0 + mr^2 \tag{22}$$

$$\mu_1 = \frac{mr}{M+m} \tag{23}$$

$$\mu_2 = \frac{mr}{J_1} \tag{24}$$

Encoder

Figure 22 shows the optical sensor used to measure the angular velocity of the motor during the experimental tests.

References

1. Balthazar JM, Mook DT, Weber HI, Brasil RM, Fenili A, Belato D, Felix J (2003) An overview on non-ideal vibrations. Meccanica 38(6):613–621
2. Bishop SR, Galvanetto U (1993) The behaviour of nonlinear oscillators subjected to ramped forcing. Meccanica 28(3):249–256
3. Dhondt G (2004) The finite element method for three-dimensional thermomechanical applications. Wiley Online Library
4. Felix JLP, Balthazar JM (2009) Comments on a nonlinear and nonideal electromechanical damping vibration absorber, sommerfeld effect and energy transfer. Nonlinear Dyn 55(1–2):1–11
5. Felix JLP, Balthazar JM, Brasil RM (2005) On saturation control of a non-ideal vibrating portal frame foundation type shear-building. J Vib Control 11(1):121–136
6. Geuzaine C, Remacle JF (2009) Gmsh: A 3-d finite element mesh generator with built-in pre-and post-processing facilities. Int J Numer Methods Eng 79(11):1309–1331
7. Gonçalves PJP, Silveira M, Pontes BR Jr, Balthazar JM (2014) The dynamic behavior of a cantilever beam coupled to a non-ideal unbalanced motor through numerical and experimental analysis. J Sound Vibration 333(20):5115–5129
8. Hairer E, Wanner G (1996) Solving ordinary differential equations II: stiff and differential-algebraic problems. Springer, Berlin
9. Kerschen G, McFarland DM, Kowtko JJ, Lee YS, Bergman LA, Vakakis AF (2007) Experimental demonstration of transient resonance capture in a system of two coupled oscillators with essential stiffness nonlinearity. J Sound Vib 299(4):822–838
10. Krasnopolskaya T (2006) Chaos in acoustic subspace raised by the sommerfeld-kononenko effect. Meccanica 41(3):299–310
11. Lee YS, Kerschen G, Vakakis AF, Panagopoulos P, Bergman L, McFarland DM (2005) Complicated dynamics of a linear oscillator with a light, essentially nonlinear attachment. Phys D: Nonlinear Phenom 204(1):41–69
12. Palacios J, Balthazar J, Brasil R (2002) On non-ideal and non-linear portal frame dynamics analysis using bogoliubov averaging method. J Braz Soc Mech Sci 24(4):257–265
13. Quinn D, Rand R, Bridge J (1995) The dynamics of resonant capture. Nonlinear Dyn 8:1–20
14. Quinn DD (1997) Resonance capture in a three degree-of-freedom mechanical system. Nonlinear Dyn 14(4):309–333
15. Sommerfeld A (1902) Beiträge zum dynamischen ausbau der festigkeitslehe. Physikal Zeitschr 3:266–286
16. Zniber A, Quinn DD (2006) Resonance capture in a damped three-degree-of-freedom system: experimental and analytical comparison. Int J Non-Linear Mech 41(10):1128–1142